JEM Journal of Experimental Medicine

ARTICLE

NK cells switch from granzyme B to death receptor–mediated cytotoxicity during serial killing

Isabel Prager[1*], Clarissa Liesche[2*], Hanna van Ooijen[3*], Doris Urlaub[1], Quentin Verron[3], Niklas Sandström[3], Frank Fasbender[1], Maren Claus[1], Roland Eils[2], Joël Beaudouin[2], Björn Önfelt[3,4], and Carsten Watzl[1]

NK cells eliminate virus-infected and tumor cells by releasing cytotoxic granules containing granzyme B (GrzB) or by engaging death receptors that initiate caspase cascades. The orchestrated interplay between both cell death pathways remains poorly defined. Here we simultaneously measure the activities of GrzB and caspase-8 in tumor cells upon contact with human NK cells. We observed that NK cells switch from inducing a fast GrzB-mediated cell death in their first killing events to a slow death receptor–mediated killing during subsequent tumor cell encounters. Target cell contact reduced intracellular GrzB and perforin and increased surface-CD95L in NK cells over time, showing how the switch in cytotoxicity pathways is controlled. Without perforin, NK cells were unable to perform GrzB-mediated serial killing and only killed once via death receptors. In contrast, the absence of CD95 on tumor targets did not impair GrzB-mediated serial killing. This demonstrates that GrzB and death receptor–mediated cytotoxicity are differentially regulated during NK cell serial killing.

Introduction

Cellular cytotoxicity is an important effector mechanism of the immune system (Golstein and Griffiths, 2018; Prager and Watzl, 2019). The ability to directly kill other cells is essential for the removal of infected or transformed cells and is therefore a central tool in the immune system's fight against viral infections and cancer. The most effective mediators of cellular cytotoxicity are $CD8^+$ CTLs and natural killer (NK) cells (Zhang and Bevan, 2011; Cerwenka and Lanier, 2016; Halle et al., 2017). It is well established that the activities of these cytotoxic lymphocytes are important for the elimination of tumors (Imai et al., 2000; Guillerey et al., 2016; Malmberg et al., 2017). Notably, modern approaches for the immunotherapy of cancer rely on enhancing the function of these cytotoxic effector cells. Checkpoint inhibitors such as antibodies against PD-1, PD-L1, or CTLA4 can enhance CTL (Curran et al., 2010) and NK cell responses (Chiossone et al., 2017) against tumors and have shown very promising clinical results (Wolchok et al., 2013). The recently approved therapy using T cells expressing a chimeric antigen receptor (CAR) T cells (June et al., 2018) or studies using CAR NK cells (Daher and Rezvani, 2018) represent another promising example of the successful use of cytotoxic effector cells to combat cancer. In addition to eliminating tumors or infected cells, cellular cytotoxicity is also important for the down-regulation of cellular immune activation, as evident by the uncontrolled immune activation in patients suffering from hemophagocytic lymphohistiocytosis (Al-Samkari and Berliner, 2018), which can be caused by defects in the cytotoxic machinery of CTLs and NK cells.

Cellular cytotoxicity is mediated by the directed release of preformed cytotoxic granules, which are lysosomal-related organelles (Stinchcombe and Griffiths, 2007; Krzewski and Coligan, 2012). The exocytosis of lytic granules is a multi-step regulated process that is initiated by the contact between the effector and the target cell (Urlaub et al., 2017), leading to the formation of an immunological synapse (IS; Davis et al., 1999). Within the IS, cell surface receptors of the cytotoxic lymphocytes can interact with their respective ligands on the target cell. Engagement of the T cell receptor is essential for CTL activation, whereas NK cell activity is regulated by a variety of different activating and inhibitory receptors (Watzl, 2014). The signals originating at the IS result in a reorganization of the actin cytoskeleton, a convergence of lytic granules to the microtubule-organizing center, and a polarization of the microtubule-organizing center toward the IS (Mace et al., 2014). Finally, lytic granules fuse with the plasma membrane and release their content into the IS.

[1]Department for Immunology, Leibniz Research Centre for Working Environment and Human Factors at TU Dortmund, Dortmund, Germany; [2]Division of Theoretical Bioinformatics, German Cancer Research Center and BioQuant Center, Heidelberg, Germany; [3]Department of Applied Physics, Science for Life Laboratory, KTH Royal Institute of Technology, Stockholm, Sweden; [4]Department of Microbiology, Tumor and Cell Biology, Karolinska Institutet, Stockholm, Sweden.

*I. Prager, C. Liesche, and H. van Ooijen contributed equally to this paper; Correspondence to Carsten Watzl: watzl@ifado.de; Joël Beaudouin: jbeaudouin@googlemail.com; Björn Önfelt: onfelt@kth.se.

Lytic granules contain the pore-forming protein perforin and several proteases called granzymes, of which granzyme B (GrzB) is the best characterized one (Chowdhury and Lieberman, 2008). Once released into the IS, granzymes are delivered into the cytosol of the target cell with the help of perforin (Law et al., 2010), while the membrane of cytotoxic lymphocytes is protected from this attack (Cohnen et al., 2013). Granzymes can be quickly delivered into the target cell through perforin pores directly at the plasma membrane (Lopez et al., 2013). Additionally, it was suggested that they enter through endocytosis of the damaged membrane and a perforin-mediated escape of granzymes from intracellular endosomes (Froelich et al., 1996; Thiery et al., 2011). Once delivered to the target cell, granzymes can initiate apoptosis by cleaving several substrates such as Bid, caspase-3, DNA-PKc, and others (Quan et al., 1996; Andrade et al., 1998; Barry et al., 2000; Sutton et al., 2000).

Besides the release of perforin and granzymes, CTL and NK cells can also present CD95L or TNF-related apoptosis-inducing ligand (TRAIL) on their surface, which activate their respective death receptors CD95/Fas and TRAIL-R1-R2 on the surface of the target cell (Rouvier et al., 1993; Kägi et al., 1994; Strasser et al., 2009). Death receptor activation induces apoptosis starting with the formation of the so-called death-inducing signaling complex (Medema et al., 1997), composed of activated death receptors and recruited FADD adaptor proteins and initiator procaspases-8–10. Activation of caspase-8 (Casp8) and -10 at the death-inducing signaling complex initiates a caspase cascade, ultimately leading to apoptosis (Peter and Krammer, 2003).

The two distinct cytotoxic mechanisms were shown to act on different time scales, with rapid granule-mediated cell death and slower CD95-induced apoptosis (Hassin et al., 2011; Li et al., 2014; Zhu et al., 2016). After apoptosis of the target cell via granule- or death receptor–mediated apoptosis, the locally attached cytotoxic lymphocyte can disengage (Netter et al., 2017) and subsequently mediate additional killing events of neighboring target cells, a process termed serial killing (Zagury et al., 1975; Isaaz et al., 1995; Bhat and Watzl, 2007; Vanherberghen et al., 2013).

While it is clear that cytotoxic lymphocytes possess two distinct effector mechanisms to kill target cells, it is unclear if and how these two mechanisms are coordinated and if they are regulated during the serial killing activity of CTL and NK cells. Both cytotoxic mechanisms are based on the activity of proteases, GrzB for granule-mediated cytotoxicity and Casp8 for death receptor–mediated apoptosis. We recently developed fluorescent localization reporters to measure protease activity in single living cells (Beaudouin et al., 2013). These reporters are based on a single fluorescent protein (e.g., monomeric GFP [mGFP]) that is fused via a cleavable linker to a nuclear export signal sequence (NES). In its uncleaved form, the reporter is excluded from the nucleus, while cleavage of the linker via a specific protease liberates the fluorescent protein, which can then diffuse into the nucleus. In contrast to other approaches (Kanno et al., 2007; Packard et al., 2007; Choi and Mitchison, 2013; Li et al., 2014; Vrazo et al., 2015), this reporter allows for the parallel detection of two different protease activities within the same target cell upon NK cell–mediated killing (Liesche et al., 2018).

Here we use live cell imaging of fluorescent localization reporters to detect GrzB and Casp8 activities in single target cells upon their killing by NK cells. We show that the two different killing mechanisms are regulated during the serial killing activity of NK cells. For their first killing events, NK cells almost exclusively use the granule-mediated pathway, resulting in very fast and thus efficient killing of target cells. This is paralleled by a loss of granule content and an increase of surface CD95L, resulting in a switch from granule- to CD95L-mediated cytotoxicity. Therefore, the last killing event is dominated by the slower death receptor–mediated apoptosis.

Results

We recently developed fluorescent localization reporters to measure protease activity in living cells (Beaudouin et al., 2013). These reporters can be used to measure GrzB activity in living tumor cells upon killing by NK cells (Liesche et al., 2018). GrzB can cleave the reporter, resulting in an increase of fluorescent signal in the nucleus. In previous experiments, we have shown that the GrzB reporter is not cleaved upon CD95-mediated apoptosis of tumor cells and that reporter cleavage can be inhibited by overexpression of the GrzB inhibitor Serpin B9 (Liesche et al., 2018) or by using EGTA to block granule-mediated killing of NK cells (unpublished data). This demonstrates that the GrzB reporter is specific and is not influenced by caspase activity.

To distinguish perforin/GrzB-mediated death from death receptor–mediated target cell killing, we used a reporter for GrzB and a reporter for Casp8 activity in the same HeLa target cell (Video 1). We have recently shown that the Casp8 reporter was specifically activated by death receptor–mediated apoptosis and that both reporters can independently and specifically detect the activity of GrzB and Casp8 within the same cell (Liesche et al., 2018). We first used the human NK cell line NK92 as effector in order to have a defined NK cell population. Surprisingly, we detected differences in how the HeLa target cells were killed by the NK92 cells (Fig. 1 A). Some target cells showed strong Casp8 activation, and others had stronger GrzB activity, whereas some cells had equal activation of both reporters (examples are shown in Fig. 1 A). To further characterize these different cleavage behaviors, we manually classified the cells into these three categories (Fig. 1 A). Cells with stronger GrzB-reporter activity died earlier within our observation time (at 49 ± 18 min; mean ± SD), while those with equal cleavage died at 60 ± 18 min, and those with stronger Casp8 activity at 111 ± 41 min of the experiment (Fig. 1 B). To more precisely measure how long it takes for the target cells to die, we determined the time from NK cell engagement to target cell death. This time span was shorter for target cells showing strong GrzB activity (19 ± 9 min) compared with the ones with strong Casp8 activity (65 ± 31 min; time span, Fig. 1 B), confirming that GrzB kills target cells faster than death receptors.

The preferential killing of target cells through either GrzB or through Casp8 may originate from cell-to-cell variation within the NK cells. Alternatively, NK cells might change their killing mechanism during the time course of our experiment. We hypothesized that during serial killing, NK cells may first kill

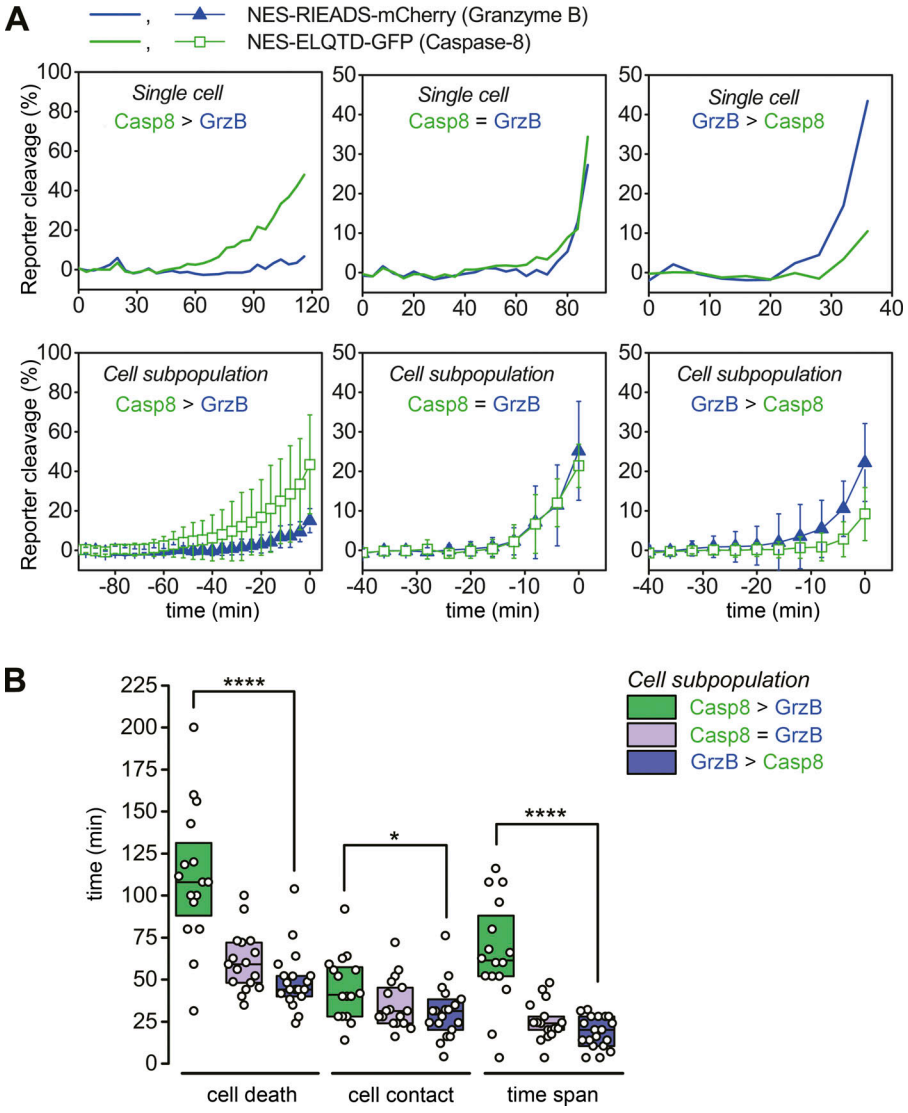

Figure 1. **Different killing kinetics of target cells showing GrzB versus Casp8 activity.** HeLa cells were cotransfected with NES-RIEADS-mCherry (for GrzB), NES-ELQTD-GFP (for Casp8), and CD48. Confocal time-lapse microscopy started immediately after NK92-C1 cell exposure (E/T = 3). From two independent experiments, 52 cells were classified according to strength of RIEADS- and ELQTD-cleavage. Three dying cells showed no (<10%) reporter cleavage and were excluded. **(A)** Responses of example single cells (upper row, real time) or of cell subpopulations (mean ± SD, time point 0 set to time of cell death) with more Casp8 than GrzB-reporter cleavage (left), equal reporter cleavage (center), or more GrzB- compared with Casp8-reporter cleavage (right), from one experiment (time resolution, 4 min). **(B)** Time of target cell death (Cell death), time point of NK cell contact with target cell (Cell contact), and the time span (from NK cell contact to target cell death) for the three cell subpopulations of both experiments is shown. ****, $P \leq 0.0001$; *, $P \leq 0.05$ (unpaired, two-tailed *t* test with Welch's correction).

through GrzB and subsequently through death receptors. To test this hypothesis, we measured the time point when an NK cell encountered a target cell by visual analysis of fluorescence images. Remarkably, while cells showing stronger GrzB activity were encountered by NK cells at 31 ± 16 min, cells showing stronger Casp8 activity were encountered later, at 45 ± 20 min (cell contact, Fig. 1 B). This would be consistent with a serial killing process of NK cells, killing their first targets predominantly through GrzB and their consecutive targets through Casp8 activation.

To further test our hypothesis, we used primary human NK cells and incubated them with the HeLa target cells expressing the Casp8 and GrzB reporters at two different effector-to-target cell ratios (E/T = 1 and E/T = 3). We expected that lowering the amount of NK cells per target cell would favor serial killing and therefore increase the number of target cells dying with stronger Casp8 activity. Using NK cells from three healthy donors, we observed the same heterogeneity in the balance of GrzB and Casp8 reporter cleavage as with NK92 cells. Similar to our previous observations (Guldevall et al., 2010; Vanherberghen et al., 2013), we also observed different morphologies of cell death: most of the cells showed a clear apoptotic phenotype, with cell shrinkage and blebbing, others shrank with little or no cell blebbing, and finally some showed no clear blebbing but a collapse of the cytoplasm (Fig. 2, A and B). Analyzing this apoptotic phenotype and the reporter cleavage, we found that a clear apoptotic phenotype was observed in 75% to 86% of cells with strong Casp8 activity and in only 48% to 56% of cells with strong GrzB activity (Fig. 2 B). The nonapoptosis-like phenotype with a collapse of the cytoplasm was mostly observed in cells with GrzB activity equal to or stronger than Casp8 activity.

The balance of GrzB versus Casp8 reporter cleavage correlated again with the timing of cell death events (Fig. 2, C–E): strong Casp8 reporter cleavage correlated with late cell death during the experiment (Fig. 2 C), late NK–target cell contact (Fig. 2 D), and long time to kill after the contact was established (Fig. 2 E). This effect was particularly visible when NK cells were more diluted (E/T = 1). Strikingly, although GrzB activity was dominant in most cell deaths that occurred at an E/T of 3, the proportion of target cells with stronger Casp8 activity was

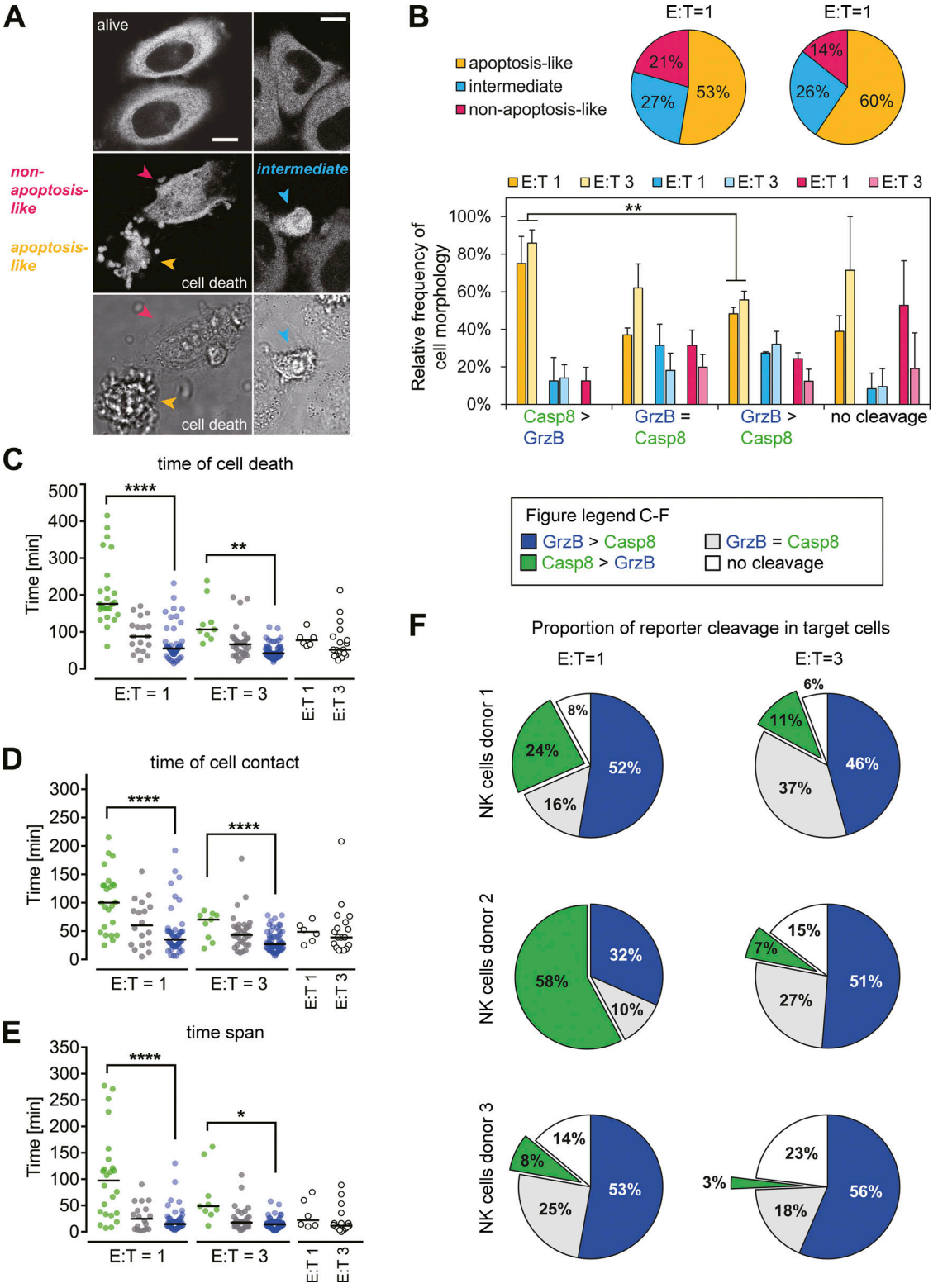

Figure 2. **Cell death morphology, GrzB, and Casp8 activity in target cells killed upon co-culture with primary NK cells.** Human primary NK cells were isolated from blood of three healthy donors. For each donor NK cell population, two experiments at different NK cell doses (E/T = 1 and E/T = 3) were performed. HeLa-CD48 target cells expressing the NES-RIEADS-mCherry (GrzB) and NES-ELQTD-GFP (Casp8) reporters were imaged over time by confocal microscopy. **(A)** Images show alive cells (top) and three different cell death morphologies that were visually distinguished (with reporter fluorescence, center; or transmission light, bottom): an apoptosis-like phenotype with cell blebbing, a non-apoptosis-like phenotype with lack of cell blebbing, and an intermediate phenotype with cell shrinkage but no or few cell blebbing. Scale bars, 10 µm. **(B)** Pie charts show the frequency of different cell death morphology for cells induced with the three donor NK cells (E/T = 1, in total 94 cells; E/T = 3, in total 119 cells). Bar graphs show this distribution as relative frequencies for cells grouped for the balance of GrzB- and Casp8-reporter cleavage and for E/T ratio (mean ± SEM, *n* = 3). **(C–E)** Plots of single cell data of the time of target death

(C), the time point of NK cell contact with target cell (D), and the time between NK cell contact and target cell death (E). The median is indicated for pooled data from three independent experiments using NK cells from three donors. **(F)** Pie charts show the proportion of reporter cleavage at the two different NK cell doses for the NK cells of each donor. ****, P ≤ 0.0001; **, P ≤ 0.01; *, P ≤ 0.05 (unpaired, two-tailed *t* test with Welch's correction).

clearly increased at an E/T of 1, where we also expect more serial killing activity (Fig. 2 F). These data would support a model where NK cells change their mode of killing over time, starting with fast granzyme-mediated killing and changing to slow death receptor–mediated killing at later stages.

With our standard video microscopy slides, we were unable to follow individual NK cells over a long period of time, as cells would enter or leave the field of view. This made it impossible to investigate serial killing events by single NK cells. To solve this problem, we used our microchip platform that enables tracking of individual NK cells (Forslund et al., 2012; Vanherberghen et al., 2013). Up to 100 target cells and 2–10 NK cells were confined in 350-µm-wide microwells, fitting within one imaging field of view, and through time-lapse imaging, we could analyze the killing sequence of all NK cells in individual microwells (Video 2). Following a single NK cell that killed five targets in a serial fashion, we observed that the first four killing events were mediated mostly by GrzB activity, whereas in the last killing event, Casp8 activity was dominant (Fig. 3 A and Video 3). When analyzing several hundred killing events of NK cells from three different healthy donors (Fig. 3 B), we observed that NK cells made almost no noncytotoxic interactions before their first kill and that in almost all cases the first killing event showed strong GrzB activity (Fig. 3 D). Only for the second kill, we observed a small fraction of target cells with dominant Casp8 activity. This fraction increased during the subsequent kills and for NK cells killing six target cells, the last kill was dominated by Casp8 activity. Interestingly, after a Casp8-mediated kill, we rarely observed another killing event (Fig. 3 B). This was not due to the fact that our observation time after the last Casp8-mediated kill was too short. In fact, we observed multiple noncytotoxic contacts of NK cells after they had eliminated their last target via Casp8 activity.

The serial killing activity differed between individual NK cells, with the majority of NK cells killing three or fewer targets (Fig. 3 B). Therefore, we repeated our analysis and differentiated between serial killers (killing more than three targets) and NK cells killing three or fewer targets (Fig. S1, A and B). For the serial killers, the first three kills were all dominated by GrzB activity with only a small fraction of targets being killed via Casp8. In contrast, for NK cells killing three or fewer targets, already the second kill showed a sizable fraction of targets with strong Casp8 activity, and the third kill was dominated by Casp8. These data support our hypothesis that NK cells switch their killing mechanism from GrzB to Casp8-mediated killing during their serial killing activity.

We also analyzed the morphology of target cell death as described in Fig. 2. Most target cells died with a clear apoptosis-like phenotype; however, especially in the first killing event, we observed a sizable fraction of target cells dying nonapoptosis-like with a collapse of the cytoplasm or a rupture of the plasma membrane (Fig. 3, C and E). Again, this was associated with GrzB activity in the target cells. Interestingly, in serial killers (killing more than three targets), the first kill was dominated by this nonapoptosis-like phenotype, whereas in NK cells killing three or fewer targets, the first kill was mostly apoptosis-like (Fig. S1, C and D). This was despite the fact that the proportion of GrzB-mediated target cell death was similar for the first target killed by all NK cells. This suggests that serial killers may release more GrzB and perforin during the first killing events, causing more nonapoptotic-like cell death (Vanherberghen et al., 2013).

To exclude that in vitro activation of the NK cells influenced their use of different killing mechanisms during serial killing, we repeated the experiments with nonactivated freshly isolated NK cells from three healthy donors. Consistent with the fact that these NK cells were less cytotoxic, we observed a maximum of four targets being killed by individual NK cells during serial killing (Fig. 3 F). However, similar to the activated NK cells, the first kill was dominated by GrzB activity, while the last kills were dominated by Casp8 activity. This demonstrates that the switch in killing mechanism during serial killing can be found in resting as well as in activated NK cells. Interestingly, most killing events of the resting NK cells had a clear apoptosis-like phenotype, which could be explained by the fact that these cells have fewer cytotoxic granules compared with activated NK cells (Fig. 3 G).

Next, we analyzed the timing of each individual cell death event and defined different steps during the killing process, starting with the first contact between the NK and the target cell (Fig. 4 A). As a next step, we wanted to determine the time point of NK cell commitment, which we defined as the time point when activating NK cell signaling occurs and the killing process is initiated. To do so, we measured Ca^{2+} flux in NK cells after target cell contact. However, while we saw a clear increase in the Ca^{2+} signal within one timeframe (time resolution, 45 s) following target cell contact, the signal stayed high for an extended period of time. This made it impossible to clearly detect additional increases in Ca^{2+} signals after subsequent contacts. Therefore, we used morphological changes (polarization of the NK cell body toward the target cell, accompanied by spreading of the NK cell membrane at the point of attachment) to determine the time point of NK cell commitment. We observed these changes within one timeframe (time resolution, 3 min) following initial cell contact, which was consistent with the Ca^{2+} data. Interestingly, this time frame was similar for GrzB- and Casp8-mediated kills (Fig. 4 B). In contrast, the time from initial contact to reporter cleavage was very short for GrzB-mediated kills (3 min), whereas it took on average 37 min for Casp8 kills (Fig. 4 C). Finally, the time span from initial contact to target cell death was also different for targets dying via Casp8 compared with cells dying via GrzB activity (Fig. 4 D). Interestingly, this time span was independent of the killing sequence. Targets that were killed via Casp8 activity in the first kill already took longer to die, whereas targets that showed GrzB activity died

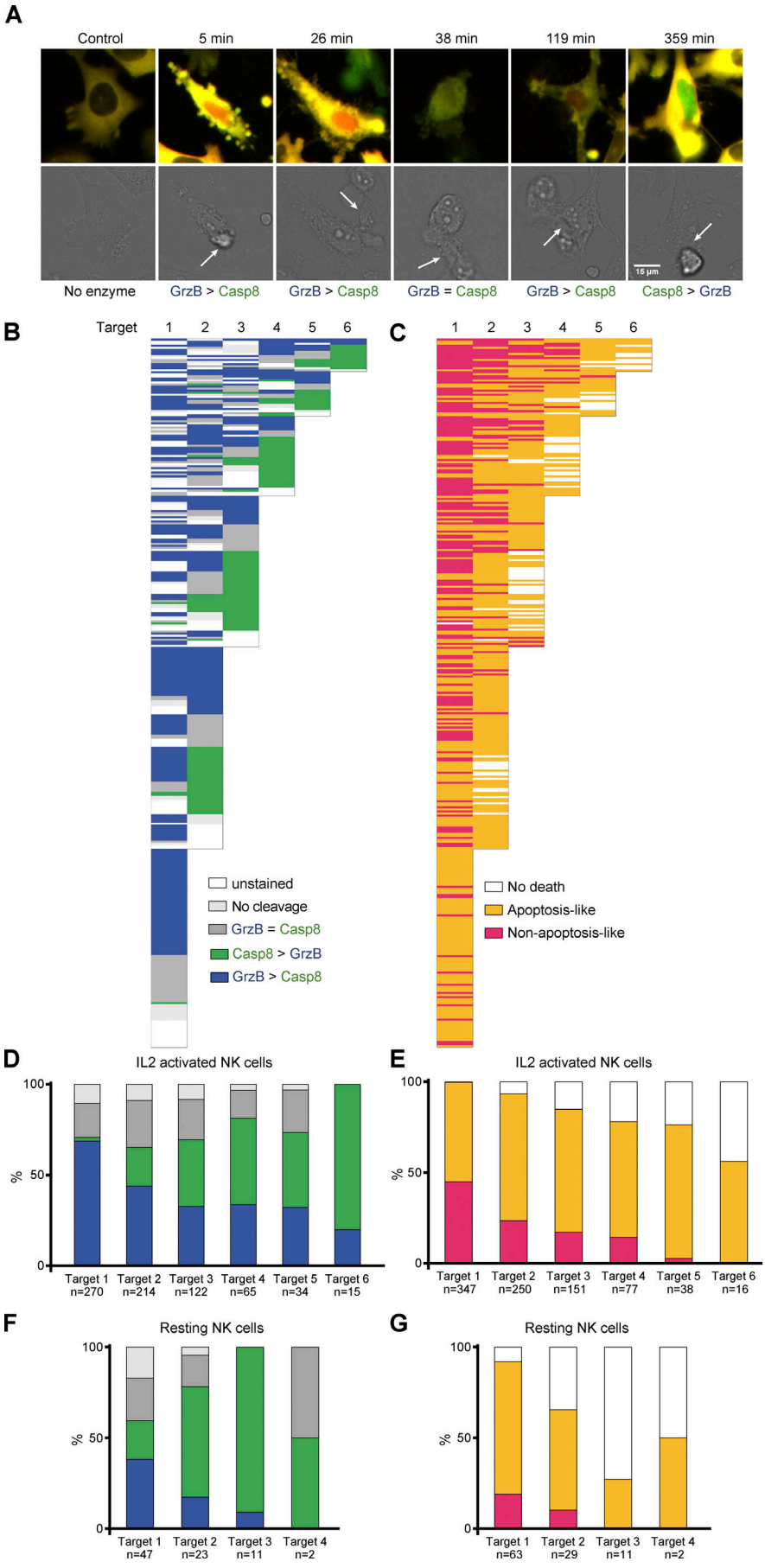

Figure 3. **NK cells differentially induce GrzB- or Casp8-mediated target cell death during serial killing.** Serial killing activity of primary human NK cells was evaluated against HeLa-CD48 cells stably expressing NES-ELQTD-GFP-T2A-NES-VGPD-mCherry. **(A–G)** Three independent experiments using IL-2–activated NK cells from three donors (A–E) and three independent experiments using resting, freshly isolated NK cells from three different donors (F and G) were conducted. A total of 347 activated and 63 resting NK cells was tracked over 15–17 h, and each of their killing events was characterized in terms of GrzB and Casp8 activity as well as morphology of cell death. **(A)** Example of five consecutive killing events by a serial killer NK cell (NK cell visualized in brightfield, arrowheads, lower row) with corresponding enzymatic activity (red and green nuclear signal indicates GrzB and Casp8 activity, respectively). Images have been background-subtracted and adjusted for brightness and contrast using ImageJ. See Video 3 for details. Scale bar, 15 µm. **(B and C)** Diagrams display the activity of GrzB and Casp8 (B) and the morphology of target cell death (C) in single killing events. Each row displays the killing sequence of one individual NK cell. Cells for which fluorescent signal could not be reliably measured are denoted by "unstained." Some target cells showed strong Casp8 reporter activity without displaying significant morphological signs of cell death during the observation period (No death). **(D–G)** Target cell deaths were categorized according to their respective number in the corresponding NK cell killing sequence. Histograms show the proportion of target cell deaths displaying activity of GrzB, Casp8, or absence of reporter cleavage (D and F) and the proportion of target cell deaths with an apoptosis-like or non-apoptosis-like phenotype (E and G). Cells showing clear enzymatic activity following an NK cell interaction, yet surviving the entire time span of the assay, are denoted by "No death." The non-apoptosis-like phenotype is classified as described in Fig. 2, and the apoptosis-like fraction also contains cells with the "intermediate" phenotype.

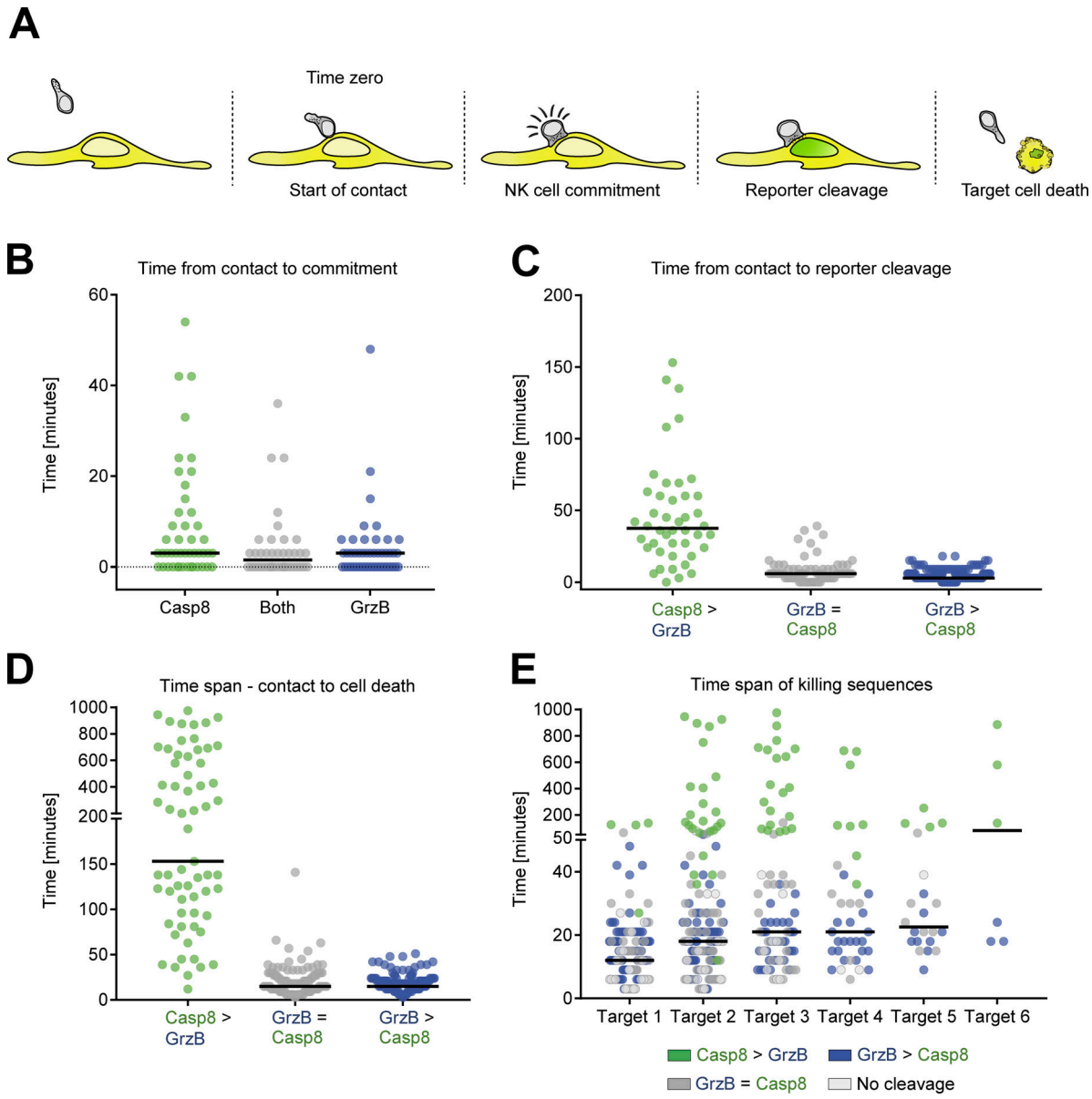

Figure 4. **Timing of killing events. (A)** Each killing event shown in Fig. 3 B was analyzed according to time of first contact, NK cell commitment, reporter cleavage, and target cell death. **(B–E)** The time span between NK cell contact and NK cell commitment (B), reporter cleavage (C), and target cell death (D and E) was plotted for individual killing events. Data were grouped according to the respective number in the corresponding NK cell killing sequence (E) or according to the reporter activity (B–D). Black lines indicate median values.

within ∼20 min even if they were killed as the sixth target (Fig. 4 E). This demonstrates that the differences in death kinetics are due to the killing pathway and not influenced by serial killing. These kinetics of NK cell–mediated cytotoxicity are consistent with a recent report that showed rapid in vivo killing by CAR T cells within ∼25 min (Cazaux et al., 2019).

To analyze why NK cells switch their killing mechanism during serial killing, we measured the amount of GrzB and perforin inside the NK cells and the amount of TRAIL and CD95L on their surface by flow cytometry. Without target cell contact, all NK cells had intracellular GrzB and perforin, but they were negative for surface CD95L (Fig. 5). As we used cytokine-activated primary human NK cells in our experiments, we detected some TRAIL on the surface of the NK cells even in the absence of target cell contact. We then incubated the NK cells with HeLa target cells and repeated the measurement after 1, 2, 3, and 4 h of coincubation. Within 1 h of target cell contact, we already observed a reduction of intracellular GrzB and perforin in the NK cells. However, this was confined to NK cells that had degranulated, as detected by surface CD107a staining (Fig. 5, A and B). NK cells that did not degranulate also did not lose any significant amount of GrzB or perforin (Fig. 5, C and D). After 4 h of target cell coincubation, the degranulating NK cells had lost most of their GrzB and perforin. CD95L was detectable on the surface of NK cells within 1 h after target cell coincubation and further increased during the incubation time. Interestingly, this

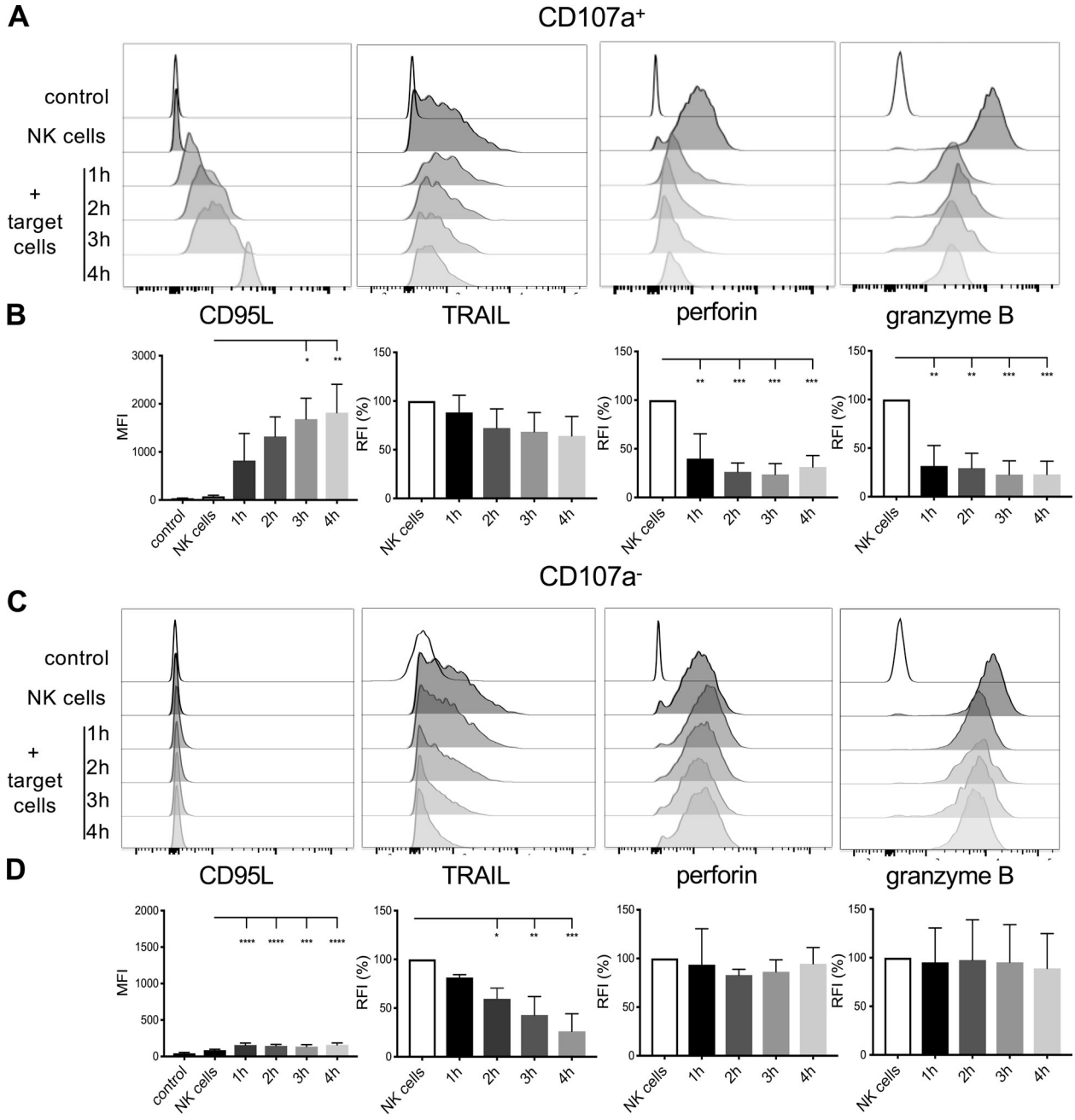

Figure 5. **Changes in granule content and surface CD95L on NK cells during serial killing.** Primary human NK cells were incubated at an E/T ratio of 2 with HeLa-CD48 cells in the presence of an anti-CD107a antibody. After the indicated times, NK cells were harvested and stained for CD45, CD95L, and TRAIL followed by intracellular staining for perforin and GrzB. Unstained NK cells (control) and stained NK cells incubated for 4 h without target cells (NK cells) were used as controls. **(A and C)** Histograms for the staining of CD95L, TRAIL, perforin, and GrzB on $CD107a^+$ (A) and $CD107a^-$ (C) NK cells (gated on $CD45^+$). **(B and D)** Summary of three independent experiments showing the mean fluorescence staining intensity (MFI) for CD95L or the relative fluorescence staining intensity (RFI, normalized to the NK cell only control) for TRAIL, perforin, and GrzB at the different time points for $CD107a^+$ (B) and $CD107a^-$ (D) NK cells. Values shown are the mean ± SD; *, $P < 0.05$; **, $P < 0.01$; ***, $P < 0.001$; ****, $P < 0.0001$ (one-way ANOVA).

was also confined to CD107a-positive, degranulating NK cells (Fig. 5). In contrast, surface expression of TRAIL was reduced after target cell coincubation, which was equally evident on degranulating and nondegranulating NK cells and potentially a result of TRAIL cleavage (Mariani and Krammer, 1998).

This suggests a mechanism by which NK cells use granule (perforin, GrzB)–mediated cytotoxicity for their first target cell encounters, which reduces the amount of perforin and GrzB during each degranulation event. At the same time, target cell contact and degranulation result in the exposure of surface CD95L. Therefore, in subsequent target cell contacts, both death receptor– and granule-mediated cytotoxicity may be operational, which would explain our finding that some target cells show equal GrzB and Casp8 activity.

When the granule content is low and CD95L surface expression is high, the final killing event would then be preferentially mediated via death receptors, resulting in strong Casp8 activity.

To further assess the contribution of both killing pathways to the serial killing activity of NK cells, we used CRISPR/Cas9 to delete perforin in primary human NK cells (Fig. 6 A). As the efficiency of the KO was only ∼30%, we generated NK cell clones and selected either perforin KO or WT clones from the same sample (Fig. 6 B). We then tested the killing of HeLa target cells by these clones by time-lapse imaging using our microchip platform. As before, we saw serial killing by the WT control clones, with initial fast GrzB-mediated killings and a switch to a slower Casp8-mediated death for the final kill (Fig. 6 C). As expected, the perforin KO NK clones only performed Casp8-mediated killing. Even though all of the first kills were now Casp8-mediated, we still observed the slow kinetics from initial contact to reporter cleavage and target cell death. However, almost all of the perforin KO NK cells only performed a single Casp8-mediated kill, even if they made additional target cell contacts afterwards (Fig. 6 D). The same phenotype was observed when we depleted perforin by treating the NK cells with concanamycin A (CMA; Fig. S2). This demonstrates that perforin is essential for the serial killing activity of NK cells.

To quantify the contribution of CD95 receptor–mediated killing, we deleted the corresponding gene from HeLa target cells using the CRISPR/Cas9 method (Fig. S3). When testing these target cells, we still observed serial killing by NK cells (Fig. 7 A). As expected, these kills were dominated by GrzB activity. Casp8-dependent kills were clearly reduced, but not absent (Fig. 7 B), possibly due to the fact that the HeLa target cells also expressed low levels of TRAIL-R2 (Fig. S3). However, in the absence of CD95, the serial killing activity of NK cells was reduced (from an average of 2.53 to 2.05 kills/NK cell), consistent with the fact that a final CD95-dependent kill was no longer possible (Fig. 7 C).

Discussion

In contrast to previously developed protease reporters for the measurement of granzyme or caspase activity that were based on luciferase (Kanno et al., 2007; Li et al., 2014), fluorophore quenching (Packard et al., 2007), or Förster resonance energy transfer imaging (Choi and Mitchison, 2013), the localization reporters used in this study (Beaudouin et al., 2013; Liesche et al., 2018) enabled simultaneous and quantitative monitoring of two protease activities in single target cells and relation of this activity to NK cell engagement and target cell death. We had previously shown that the GrzB reporter is specific for granule-mediated cytotoxicity, as it was not activated during death receptor–mediated apoptosis, and that the Casp8 reporter was specific for death receptor signaling, as it was not activated by purely granule-mediated killing (Liesche et al., 2018). We used GrzB activity as a readout for granule-mediated cytotoxicity. However, it is likely that the activities of granzyme A and other granzymes also contribute to this killing mechanism (Chowdhury and Lieberman, 2008).

We observed different kinetics for granule- and death receptor–mediated cytotoxicity. While the time from initial contact to NK cell commitment was identical for both killing pathways, the time span from NK cell contact to reporter cleavage and cell death was much longer for Casp8-mediated kills, consistent with previous reports (Zhu et al., 2016). The difference in time to reporter cleavage may be explained by the fact that death receptor activation involves receptor clustering, recruitment of the adaptor protein FADD, and the binding of procaspase-8, which then results in Casp8 processing and activation. In contrast, granule-mediated killing is initiated by the direct delivery of an already active GrzB into the cytoplasm of the target cell. Additionally, even once Casp8 is activated, the time to cell death takes much longer compared with GrzB-induced killing. Importantly, these differences in cell death kinetics were not related to the order in which the cell death occurred during serial killing. This suggests that the kinetic differences are inherent to the individual cell death pathway.

Additionally, the morphology of cell death differed between the two cell death pathways. Casp8 activation was clearly associated with apoptosis, showing the classical features such as cell condensation and membrane blebbing. In contrast, GrzB-mediated cell death was sometimes nonapoptotic-like, with membrane rupture and necrotic phenotypes. This could be due to an induction of pyroptosis mediated by activated caspase-3 as previously reported (Rogers et al., 2017; Wang et al., 2017). Alternatively, this could be caused by the amount of perforin and GrzB released by the NK cells (Backes et al., 2018). Although it was recently shown that the degranulation of as little as two to four granules is sufficient to cause cell death, it was also reported that NK cells release ∼10% of their total granules in a single killing event (Gwalani and Orange, 2018). Therefore, the amount of perforin release could be sufficient to induce nonapoptotic cell death. Interestingly, serial-killing NK cells were much more likely to cause such a nonapoptotic cell death in their first killing events compared with NK cells killing only one or two targets or compared with resting NK cells. This suggests that serial killers may release more granular content per killing event (Vanherberghen et al., 2013). This could be due to either more granules being released for each killing event or a higher granule content in serial killer NK cells, as an increase of dense-core secretory granules was recently reported to be associated with better NK cell effector functions (Goodridge et al., 2019).

Our data show that NK cells switch their killing mechanism during serial killing. In cells that were killed at early stages, Casp8 activity was very low, yet not absent. Thus, death receptor signaling was possibly initiated simultaneously with granzyme activity (Hassin et al., 2011). However, the fast and efficient granule-mediated cell death was likely dominant over the slower death receptor pathway. Only after depletion of the majority of the granules and increased concentrations of surface CD95L, the Casp8 pathway became more prominent so that the final kill was dominated by death receptor–mediated apoptosis. Gradual loss of perforin and GrzB activity may thus be functionally compensated by death receptor signaling to ensure effective cellular cytotoxicity. Interestingly, even after extensive serial killing, there was still perforin and GrzB detectable inside the NK cells,

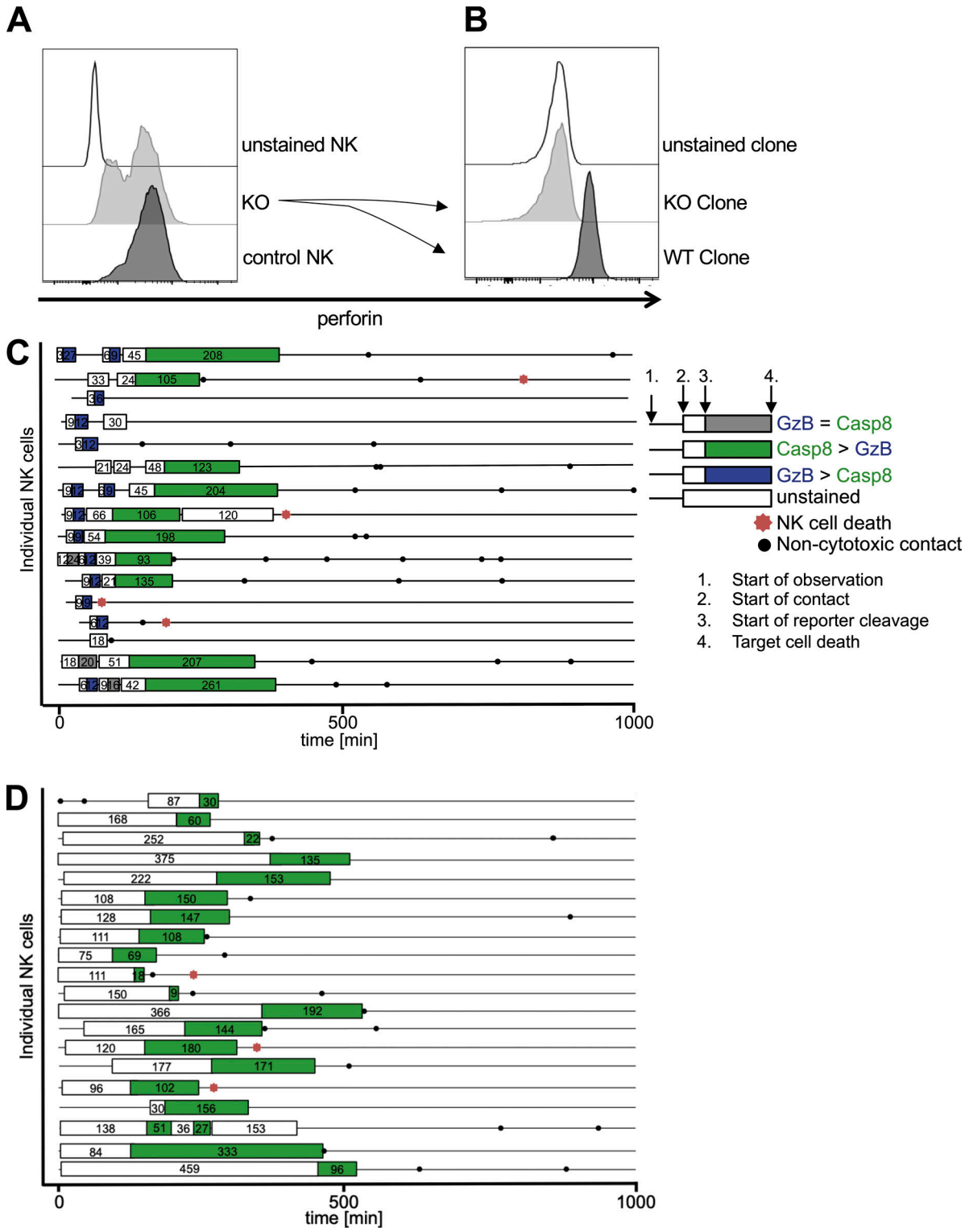

Figure 6. **Perforin is essential for NK cell serial killing. (A)** Intracellular FACS staining of perforin in human NK cells before (control) and after CRISPR/Cas9-mediated KO. **(B)** Example for intracellular perforin staining in KO and WT clones. **(C)** Perforin WT (C) and KO (D) NK cell clones (NK cells from two independent clones each) were evaluated against HeLa-CD48 cells stably expressing NES-ELQTD-GFP-T2A-NES-VGPD-mCherry. NK cells were tracked over 15–17 h, and each of their killing events was characterized in terms of GrzB and Casp8 activity as well as the kinetics of reporter cleavage and cell death.

which is consistent with the finding that NK cells lose ∼10% of their granules per killing event (Gwalani and Orange, 2018). Therefore, other factors such as down-regulation or shedding of activating receptors (Sandusky et al., 2006; Srpan et al., 2018) and attenuation of signaling events may be additional factors that limit serial killing. We have previously shown that the loss

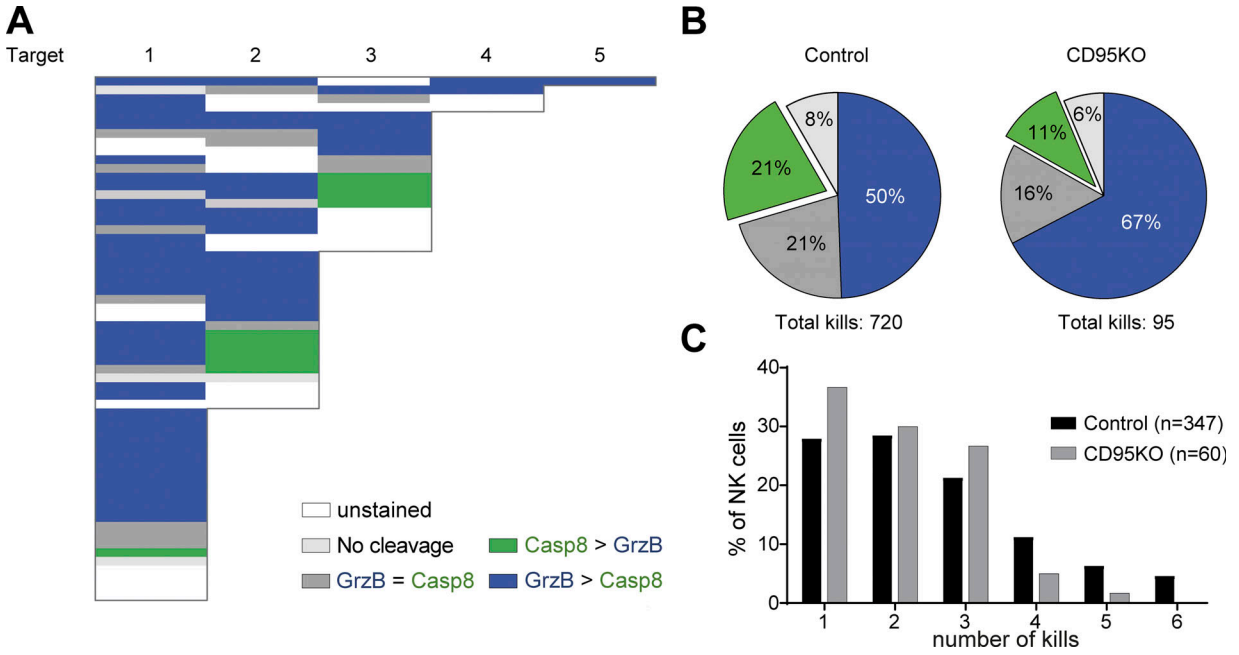

Figure 7. **Serial killing of CD95KO targets.** Serial killing activity of primary human NK cells was evaluated against CD95KO HeLa-CD48-NES-ELQTD-GFP-T2A-NES-VGPD-mCherry targets. Three independent experiments using IL-2–activated NK cells from three donors were conducted. A total of 60 NK cells were tracked over 15–17 h, and each of their killing events was characterized in terms of GrzB and Casp8 activity. **(A)** Diagram displaying the activity of GrzB and Casp8 in single killing events. Each row shows the killing sequence of one individual NK cell. **(B)** Relative distribution of reporter activity of all killing events for control and CD95KO HeLa targets. **(C)** Relative distribution of NK cells killing one to six different control or CD95KO HeLa targets.

of perforin and GrzB during serial killing can be restored within 2 d by IL-2 or IL-15 treatment (Bhat and Watzl, 2007). However, it is unclear if such a replenishment of granules can occur within a tumor environment. Alternatively, a recent report showed that switching the activating receptor to stimulate NK cell cytotoxicity could restore perforin secretion (Srpan et al., 2018). Treatments that would favor a replenishment of granules or upregulate additional ligands for activating NK cell receptors could enhance the efficiency of cytotoxic lymphocyte-based therapies.

GrzB and CD95-ligand are localized in distinct vesicular compartments inside human NK cells and CTLs (Schmidt et al., 2008, 2011). Interestingly, in our experiments, CD95L surface expression was confined to CD107a$^+$-degranulating NK cells. Therefore, while only cells that degranulate their lytic granules also mobilize CD95L-containing vesicles, the degranulation of these different vesicles seems to be differentially regulated (Kassahn et al., 2009) so that death receptor signaling serves as a back-up mechanism when perforin and GrzB levels are exhausted. In line with this, we saw that the last killing event of individual NK cells was dominated by Casp8 activity, and we observed a decrease in serial killing when using CD95KO HeLa cells. Interestingly, after a Casp8-mediated kill, we rarely observed another killing event by the NK cell. Even when NK cells were depleted of perforin, leading to the first target being killed through Casp8 activation, we did not observe additional kills. This raises the question of why NK cells do not mediate efficient serial killing using death receptors. While it appears that CD95L accumulates on the NK cell surface following degranulation, it may not be possible to concentrate enough CD95L in the contact area with a new target cell to induce cytotoxicity. Additionally, surface CD95L may be cleaved within the IS by metalloproteinases (Mariani et al., 1995), which would reduce its concentration at the NK cell surface. However, more experiments are needed to sufficiently explain this interesting finding.

Both NK cells and CTLs can kill several target cells in a serial manner (Bhat and Watzl, 2007; Choi and Mitchison, 2013; Vanherberghen et al., 2013), and both cytotoxic lymphocytes can use granule and death receptor–mediated killing pathways. While we only investigated NK cell serial killing here, it is tempting to speculate that a similar switch between cytotoxicity pathways also happens in CTLs. In addition to peripheral blood NK cells, several distinct populations of NK cells have been described in tissues (Björkström et al., 2016). Liver NK cells, for example, seem to use more TRAIL-mediated cytotoxicity and possess larger amounts of granzyme K (Moroso et al., 2010). We recently described reporters for the different granzymes (Liesche et al., 2018), and it will be interesting to compare the cytotoxicity pathways of different NK cell populations. Also, the tumor target cell will likely influence the cytotoxicity pathways. We used HeLa cells expressing CD48, the ligand for the activating receptor 2B4. However, we obtained similar results using HeLa cells without CD48 and using MDA-MB-468 breast carcinoma cells (Liesche et al., 2018). As these tumor cell lines express different ligands for activating NK cell receptors, it suggests that our findings are not restricted to one specific NK cell activation pathway. Indeed, all activating NK cell receptors can induce NK cell degranulation. However, while practically all tumor cells are sensitive to granule-mediated killing, death receptor–mediated apoptosis requires the presence of CD95/Fas or TRAIL-R1/2 on the surface of the tumor cells. Therefore, the

switch from granule- to death receptor–mediated cytotoxicity will not result in additional killings of death receptor–negative tumors, as seen with the CD95KO targets. In contrast, it could even induce fratricide of neighboring NK or CTLs (Li et al., 2002).

We believe that our insights into the killing mechanism and death kinetics of tumor cells by human NK cells are valuable for the design of cancer immunotherapies, where cytotoxic lymphocytes hold a great potential as tumor-targeting effectors.

Materials and methods

Cell culture, cell lines, and cytokines

Unless stated otherwise, all media and supplements were from Gibco/Thermo Fisher Scientific. Human NK cells were isolated from peripheral blood mononuclear cells using the Dynabeads Untouched Human NK Cell kit (Thermo Fisher Scientific) according to the manufacturer's instructions. NK cells were between 90 and 99% $CD3^-$, $CD56^+$, and $NKp46^+$ as assessed by flow cytometry. NK cells were expanded in 96-well round-bottom plates (Nunc) with irradiated K562-mbIL15-41BBL feeder cells (gift from Dario Campana; St. Jude Children's Research Hospital, Memphis, TN) in IMDM Glutamax supplemented with 10% FCS and 1% penicillin/streptomycin, IL-2 (100 U/ml; National Institutes of Health Cytokine Repository), and IL-15 (5 ng/ml; PAN-Biotech) at 37°C in a humidified 5% CO_2 incubator. IL-21 (100 ng/ml; Miltenyi Biotec) was added on the first day. For microwell microscopy, human NK cells were isolated from peripheral blood mononuclear cells using the NK Xell Isolation Kit (Miltenyi Biotec) according to the manufacturer's instructions. NK cells were cultured in RPMI 1640 cell culture media (Sigma-Aldrich) supplemented with 10% human serum (blood bank, Karolinska Hospital), 1% penicillin/streptomycin, 2 mM L-glutamine, 1× nonessential amino acids, and 1 mM sodium pyruvate (all from Sigma-Aldrich). Resting NK cells were cultured overnight, and IL-2–activated NK cells were supplemented with 100 U/ml of IL-2 (Peprotech) and used within 6–9 d of culture. All blood donors were healthy and gave their informed consent.

To create NK cell clones, we cultured single NK cells with 50,000 irradiated K562-mbIL15-41BBL feeder cells and IL-2 (100 U/ml) in 96-well U-bottom plates. After 1 wk, the cells were restimulated with 50,000 irradiated K562-mbIL15-41BBL feeder cells, and wells with expanded NK cell clones were analyzed by flow cytometry after 14 d.

HeLa cells were stably transfected with CD48 and/or the NES-ELQTD-mGFP-T2A-NES-VGPD-mCherry reporter. Transfected cells were maintained in DMEM containing 10% FCS and 1% penicillin/streptomycin supplemented with 0.5 µg/ml puromycin and 1 mg/ml G418 at 37°C in a humidified 5% CO_2 incubator. Alternatively, HeLa cells were transiently transfected with NES-RIEADS-mCherry, NES-ELQTD-mGFP, and CD48 plasmids using jetPRIME transfection reagent (Polyplus-transfection). HeLa cells showed homogenous expression of Bcl-2, BID, Serpin B9, and XIAP, excluding heterogeneity in their cell death resistance.

CRISPR/Cas9-mediated KOs

TrueCut Cas9 Protein v2 (120 pmol) was mixed with two TrueGuide synthetic guide RNAs (150 pmol each; perforin: 5′-ATCCGCAACGACTGGAAGGT-3′ and 5′-CTGTGAAAATGC CCTACAGG-3′, CD95: 5′-GATCCAGATCTAACTTGGGG-3′ and 5′-TGCACTTGGTATTCTGGGTC-3′) and delivered into primary human NK or HeLa cells via nucleofection (4D-Nucleofector; Lonza). After 7 d, the cells were analyzed by flow cytometry (anti-perforin clone dG9, BioLegend; anti-CD95 clone CX2, BD Biosciences) and either FACS-sorted (HeLa-CD95KO) or cloned (perforin KO NK cells) to obtain KO cells.

Flow cytometry

The frequency of death ligand–expressing and degranulating NK cells was examined by multi-parameter extracellular and intracellular staining. NK and HeLa-CD48 target cells were incubated at an E/T ratio of 2 for different time periods (1–4 h) in the presence of a PE/Cy5-conjugated anti-CD107a antibody (clone H4A3; BD Biosciences). NK cells were separated from adherent target cells by collecting the supernatant and washing the wells with PBS. NK cells were stained with Alexa Fluor 700–conjugated anti-CD45 antibody (clone HI30; BD Biosciences) and biotinylated anti-CD95L (clone NOK-1; BD Biosciences followed by streptavidin-PE) or PE-conjugated anti-TRAIL (clone RIK-2; BioLegend). For intracellular staining, NK cells were fixed with 2% paraformaldehyde and permeabilized with Permeabilizing Solution 2 (BD Bioscience) and stained with FITC-conjugated anti-perforin antibody (clone dG9; BioLegend) and anti-GrzB antibody conjugated to Pacific Blue (clone GB11; BioLegend). TRAIL-receptor 1/2 were stained on HeLa cells using PE conjugated TRAIL-R1/R2 (clone HS101/HS201; AdipoGen) antibodies. Cells were measured on a BD LSRFortessa flow cytometer, and data were analyzed using FlowJo software (FlowJo).

Western blotting

NK cells were treated with 50 nM CMA or DMSO for three hours at 37°C. Cells were lysed as previously described (Fasbender et al., 2017) and analyzed by Western blotting using the following antibodies: anti-human perforin (Pf-344; MabTech), β-actin (4967; Cell Signaling), and anti-CD107a (H4A3; BD Biosciences).

Microscopy

Time-lapse microscopy was performed with the TCS SP5 confocal laser scanning microscope (Leica Microsystems CMS) equipped with a 63×/1.4 OIL, HCX PL APO CS objective. Fluorescence of GFP and mCherry was acquired in line sequential mode. For mCherry, we used the helium–neon laser (561 nm), detection range 600–660 nm. For GFP, we used the argon laser (488 nm), detection range 500–560 nm. Alternatively, we used an EVOS FL Auto Imaging System (Thermo Fisher Scientific) equipped with a 60×/1.42 OIL, Plan Apochromat objective and a on stage incubator (37°C, 5% CO_2, and humidity >80%) and different EVOS LED light cubes (GFP, RFP, transmission). Cells were imaged in 8-well ibidi chambers (ibidi). The time-resolution was ∼2–4 min depending on the number of imaged fields and microscopy settings.

For imaging of serial killing events, HeLa-CD48 cells that stably express NES-ELQTD-GFP-T2A-NES-VGPD-mCherry were seeded onto a silicon-glass microchip containing 100 350-µm-wide wells (Frisk et al., 2011). HeLa cells were left to adhere to the microchip glass bottom overnight. The following day, NK cells were added to the microchip, resulting in a stochastic distribution of ∼2–10 NK cells and 40–100 target cells per microwell. Time-lapse live-cell microscopy was immediately started using a Zeiss Axio Observer Z1 7 microscope equipped with a 20×/0.8 Plan-Apochromat objective and an incubation chamber with environmental control (37°C, 5% CO_2, and humidity device S1). EGFP and mCherry were excited using the Colibri 7 LED-module 475 (filter set 90 HE LED) and 567 (filter set 91 HE LED), respectively, and brightfield was acquired using the TL LED module. Images were acquired every 3 min for 15–17 h using a Hamamatsu ORCA-flash 4.0 camera.

Image analysis and statistics

Images were analyzed using ImageJ essentially as described (Liesche et al., 2018). In short, by quantifying the spatial redistribution of the fluorescence signal from the cytoplasm to the nucleus, reporter cleavage can be calculated. Image analysis was done by generation of an image stack from time series data, background subtraction and measurement of the mean fluorescence signal in a region of interest representing the cell nucleus. To estimate the extent of substrate cleavage, this nuclear fluorescence signal intensity (I) is normalized to the cytosolic one. This normalization was performed for each time point (t), which has the advantage of correcting for potential photobleaching over time:

$$I_{nucleus}^{normalized}(t) = \frac{I_{nucleus}(t)}{I_{cytosol}(t)}.$$

For microchip experiments, normalization was performed using the cytosolic signal of the target cell at a single time point before NK cell attachment. This was done as photobleaching was minor and its effect on the measurements was negligible.

Cell death of HeLa target cells could be determined by the change of the cell's morphology. While cell rounding was often observed, we also found cells showing shrinkage without typical apoptotic blebbing. Changes in target cell morphology were detected by monitoring target cells by time-lapse microscopy in the fluorescence and transmission light channels.

ANOVA analysis and unpaired, two-tailed t tests were performed using GraphPad Prism software. When variances between groups differed significantly, the test was applied with Welch's correction. Data groups were considered not significantly different when $P > 0.05$. Otherwise they were considered significantly different with ****, $P \le 0.0001$; ***, $P \le 0.001$; **, $P \le 0.01$; or *, $P \le 0.05$.

Online supplemental material

Fig. S1 displays a difference in the killing pathway and the death phenotype of serial-killing NK cells versus nonserial-killing NK cells. Fig. S2 depicts the killing activity of NK cells treated with CMA, which depletes mature perforin and thereby blocks GrzB-mediated killing events. These NK cells only kill once via Casp8 activity. Fig. S3 shows the surface staining of CD95, TRAIL-R1, and TRAIL-R2 in HeLa target cells with and without CRISPR/Cas9-mediated deletion of CD95. Video 1 shows an example of the detection of GrzB and Casp8 activity during NK cell–mediated killing of a HeLa-CD48 target stably expressing NES-ELQTD-GFP-T2A-NES-VGPD-mCherry. The red fluorescence in the nucleus indicates that the target cell dies via GrzB activity. Video 2 shows an example of a 17-h time-lapse video using a 350-µm-wide microwell containing HeLa-CD48/NES-ELQTD-GFP-T2A-NES-VGPD-mCherry cells and four NK cells (not fluorescent). NK cells tracks are marked by different colors, and killing events are indicated by red crosses. Video 3 shows five consecutive killing events caused by a serial killer NK cell as shown in Fig. 3 A.

Acknowledgments

We thank Mina Sandusky for help with the CRISPR/Cas9 system.

This work was supported in part by the Initiative and Networking Fund of the Helmholtz Association within the Helmholtz Alliance on Systems Biology/SBCancer. C. Watzl is supported by the Deutsche Forschungsgemeinschaft (DFG, WA-1552/8-1). B. Önfelt is funded by the Swedish Foundation for Strategic Research (SBE13-0092), the Swedish Cancer Foundation (2015-05268), and the Swedish Research Council (CAN 2016/730).

The authors declare no competing financial interests.

Author contributions: I. Prager, C. Liesche, and H. van Ooijen designed the study, performed experiments, analyzed the data, and helped write the paper. D. Urlaub, Q. Verron, N. Sandström, F. Fasbender, and M. Claus performed experiments and analyzed data. R. Eils supervised the work. J. Beaudouin and B. Önfelt supervised the work and helped write the paper. C. Watzl designed the study, supervised the work, and wrote the paper.

Submitted: 31 July 2018
Revised: 12 November 2018
Accepted: 14 June 2019

References

Al-Samkari, H., and N. Berliner. 2018. Hemophagocytic Lymphohistiocytosis. *Annu. Rev. Pathol.* 13:27–49. https://doi.org/10.1146/annurev-pathol-020117-043625

Andrade, F., S. Roy, D. Nicholson, N. Thornberry, A. Rosen, and L. Casciola-Rosen. 1998. Granzyme B directly and efficiently cleaves several downstream caspase substrates: implications for CTL-induced apoptosis. *Immunity*. 8:451–460. https://doi.org/10.1016/S1074-7613(00)80550-6

Backes, C.S., K.S. Friedmann, S. Mang, A. Knörck, M. Hoth, and C. Kummerow. 2018. Natural killer cells induce distinct modes of cancer cell death: Discrimination, quantification, and modulation of apoptosis, necrosis, and mixed forms. *J. Biol. Chem.* 293:16348–16363. https://doi.org/10.1074/jbc.RA118.004549

Barry, M., J.A. Heibein, M.J. Pinkoski, S.F. Lee, R.W. Moyer, D.R. Green, and R.C. Bleackley. 2000. Granzyme B short-circuits the need for caspase 8 activity during granule-mediated cytotoxic T-lymphocyte killing by

directly cleaving Bid. *Mol. Cell. Biol.* 20:3781–3794. https://doi.org/10.1128/MCB.20.11.3781-3794.2000

Beaudouin, J., C. Liesche, S. Aschenbrenner, M. Hörner, and R. Eils. 2013. Caspase-8 cleaves its substrates from the plasma membrane upon CD95-induced apoptosis. *Cell Death Differ.* 20:599–610. https://doi.org/10.1038/cdd.2012.156

Bhat, R., and C. Watzl. 2007. Serial killing of tumor cells by human natural killer cells--enhancement by therapeutic antibodies. *PLoS One.* 2:e326. https://doi.org/10.1371/journal.pone.0000326

Björkström, N.K., H.G. Ljunggren, and J. Michaëlsson. 2016. Emerging insights into natural killer cells in human peripheral tissues. *Nat. Rev. Immunol.* 16:310–320. https://doi.org/10.1038/nri.2016.34

Cazaux, M., C.L. Grandjean, F. Lemaître, Z. Garcia, R.J. Beck, I. Milo, J. Postat, J.B. Beltman, E.J. Cheadle, and P. Bousso. 2019. Single-cell imaging of CAR T cell activity in vivo reveals extensive functional and anatomical heterogeneity. *J. Exp. Med.* 216:1038–1049. https://doi.org/10.1084/jem.20182375

Cerwenka, A., and L.L. Lanier. 2016. Natural killer cell memory in infection, inflammation and cancer. *Nat. Rev. Immunol.* 16:112–123. https://doi.org/10.1038/nri.2015.9

Chiossone, L., M. Vienne, Y.M. Kerdiles, and E. Vivier. 2017. Natural killer cell immunotherapies against cancer: checkpoint inhibitors and more. *Semin. Immunol.* 31:55–63. https://doi.org/10.1016/j.smim.2017.08.003

Choi, P.J., and T.J. Mitchison. 2013. Imaging burst kinetics and spatial coordination during serial killing by single natural killer cells. *Proc. Natl. Acad. Sci. USA.* 110:6488–6493. https://doi.org/10.1073/pnas.1221312110

Chowdhury, D., and J. Lieberman. 2008. Death by a thousand cuts: granzyme pathways of programmed cell death. *Annu. Rev. Immunol.* 26:389–420. https://doi.org/10.1146/annurev.immunol.26.021607.090404

Cohnen, A., S.C. Chiang, A. Stojanovic, H. Schmidt, M. Claus, P. Saftig, O. Janßen, A. Cerwenka, Y.T. Bryceson, and C. Watzl. 2013. Surface CD107a/LAMP-1 protects natural killer cells from degranulation-associated damage. *Blood.* 122:1411–1418. https://doi.org/10.1182/blood-2012-07-441832

Curran, M.A., W. Montalvo, H. Yagita, and J.P. Allison. 2010. PD-1 and CTLA-4 combination blockade expands infiltrating T cells and reduces regulatory T and myeloid cells within B16 melanoma tumors. *Proc. Natl. Acad. Sci. USA.* 107:4275–4280. https://doi.org/10.1073/pnas.0915174107

Daher, M., and K. Rezvani. 2018. Next generation natural killer cells for cancer immunotherapy: the promise of genetic engineering. *Curr. Opin. Immunol.* 51:146–153. https://doi.org/10.1016/j.coi.2018.03.013

Davis, D.M., I. Chiu, M. Fassett, G.B. Cohen, O. Mandelboim, and J.L. Strominger. 1999. The human natural killer cell immune synapse. *Proc. Natl. Acad. Sci. USA.* 96:15062–15067. https://doi.org/10.1073/pnas.96.26.15062

Fasbender, F., M. Claus, S. Wingert, M. Sandusky, and C. Watzl. 2017. Differential Requirements for Src-Family Kinases in SYK or ZAP70-Mediated SLP-76 Phosphorylation in Lymphocytes. *Front. Immunol.* 8:789. https://doi.org/10.3389/fimmu.2017.00789

Forslund, E., K. Guldevall, P.E. Olofsson, T. Frisk, A.E. Christakou, M. Wiklund, and B. Onfelt. 2012. Novel Microchip-Based Tools Facilitating Live Cell Imaging and Assessment of Functional Heterogeneity within NK Cell Populations. *Front. Immunol.* 3:300. https://doi.org/10.3389/fimmu.2012.00300

Frisk, T.W., M.A. Khorshidi, K. Guldevall, B. Vanherberghen, and B. Önfelt. 2011. A silicon-glass microwell platform for high-resolution imaging and high-content screening with single cell resolution. *Biomed. Microdevices.* 13:683–693. https://doi.org/10.1007/s10544-011-9538-2

Froelich, C.J., K. Orth, J. Turbov, P. Seth, R. Gottlieb, B. Babior, G.M. Shah, R.C. Bleackley, V.M. Dixit, and W. Hanna. 1996. New paradigm for lymphocyte granule-mediated cytotoxicity. Target cells bind and internalize granzyme B, but an endosomolytic agent is necessary for cytosolic delivery and subsequent apoptosis. *J. Biol. Chem.* 271:29073–29079. https://doi.org/10.1074/jbc.271.46.29073

Golstein, P., and G.M. Griffiths. 2018. An early history of T cell-mediated cytotoxicity. *Nat. Rev. Immunol.* 18:527–535. https://doi.org/10.1038/s41577-018-0009-3

Goodridge, J.P., B. Jacobs, M.L. Saetersmoen, D. Clement, Q. Hammer, T. Clancy, E. Skarpen, A. Brech, J. Landskron, C. Grimm, et al. 2019. Remodeling of secretory lysosomes during education tunes functional potential in NK cells. *Nat. Commun.* 10:514. https://doi.org/10.1038/s41467-019-08384-x

Guillerey, C., N.D. Huntington, and M.J. Smyth. 2016. Targeting natural killer cells in cancer immunotherapy. *Nat. Immunol.* 17:1025–1036. https://doi.org/10.1038/ni.3518

Guldevall, K., B. Vanherberghen, T. Frisk, J. Hurtig, A.E. Christakou, O. Manneberg, S. Lindström, H. Andersson-Svahn, M. Wiklund, and B. Önfelt. 2010. Imaging immune surveillance of individual natural killer cells confined in microwell arrays. *PLoS One.* 5:e15453. https://doi.org/10.1371/journal.pone.0015453

Gwalani, L.A., and J.S. Orange. 2018. Single Degranulations in NK Cells Can Mediate Target Cell Killing. *J. Immunol.* 200:3231–3243. https://doi.org/10.4049/jimmunol.1701500

Halle, S., O. Halle, and R. Förster. 2017. Mechanisms and Dynamics of T Cell-Mediated Cytotoxicity In Vivo. *Trends Immunol.* 38:432–443. https://doi.org/10.1016/j.it.2017.04.002

Hassin, D., O.G. Garber, A. Meiraz, Y.S. Schiffenbauer, and G. Berke. 2011. Cytotoxic T lymphocyte perforin and Fas ligand working in concert even when Fas ligand lytic action is still not detectable. *Immunology.* 133:190–196. https://doi.org/10.1111/j.1365-2567.2011.03426.x

Imai, K., S. Matsuyama, S. Miyake, K. Suga, and K. Nakachi. 2000. Natural cytotoxic activity of peripheral-blood lymphocytes and cancer incidence: an 11-year follow-up study of a general population. *Lancet.* 356:1795–1799. https://doi.org/10.1016/S0140-6736(00)03231-1

Isaaz, S., K. Baetz, K. Olsen, E. Podack, and G.M. Griffiths. 1995. Serial killing by cytotoxic T lymphocytes: T cell receptor triggers degranulation, refilling of the lytic granules and secretion of lytic proteins via a non-granule pathway. *Eur. J. Immunol.* 25:1071–1079. https://doi.org/10.1002/eji.1830250432

June, C.H., R.S. O'Connor, O.U. Kawalekar, S. Ghassemi, and M.C. Milone. 2018. CAR T cell immunotherapy for human cancer. *Science.* 359:1361–1365. https://doi.org/10.1126/science.aar6711

Kägi, D., F. Vignaux, B. Ledermann, K. Bürki, V. Depraetere, S. Nagata, H. Hengartner, and P. Golstein. 1994. Fas and perforin pathways as major mechanisms of T cell-mediated cytotoxicity. *Science.* 265:528–530. https://doi.org/10.1126/science.7518614

Kanno, A., Y. Yamanaka, H. Hirano, Y. Umezawa, and T. Ozawa. 2007. Cyclic luciferase for real-time sensing of caspase-3 activities in living mammals. *Angew. Chem. Int. Ed. Engl.* 46:7595–7599. https://doi.org/10.1002/anie.200700538

Kassahn, D., U. Nachbur, S. Conus, O. Micheau, P. Schneider, H.U. Simon, and T. Brunner. 2009. Distinct requirements for activation-induced cell surface expression of preformed Fas/CD95 ligand and cytolytic granule markers in T cells. *Cell Death Differ.* 16:115–124. https://doi.org/10.1038/cdd.2008.133

Krzewski, K., and J.E. Coligan. 2012. Human NK cell lytic granules and regulation of their exocytosis. *Front. Immunol.* 3:335. https://doi.org/10.3389/fimmu.2012.00335

Law, R.H., N. Lukoyanova, I. Voskoboinik, T.T. Caradoc-Davies, K. Baran, M.A. Dunstone, M.E. D'Angelo, E.V. Orlova, F. Coulibaly, S. Verschoor, et al. 2010. The structural basis for membrane binding and pore formation by lymphocyte perforin. *Nature.* 468:447–451. https://doi.org/10.1038/nature09518

Li, J.H., D. Rosen, P. Sondel, and G. Berke. 2002. Immune privilege and FasL: two ways to inactivate effector cytotoxic T lymphocytes by FasL-expressing cells. *Immunology.* 105:267–277. https://doi.org/10.1046/j.1365-2567.2002.01380.x

Li, J., S.K. Figueira, A.C. Vrazo, B.F. Binkowski, B.L. Butler, Y. Tabata, A. Filipovich, M.B. Jordan, and K.A. Risma. 2014. Real-time detection of CTL function reveals distinct patterns of caspase activation mediated by Fas versus granzyme B. *J. Immunol.* 193:519–528. https://doi.org/10.4049/jimmunol.1301668

Liesche, C., P. Sauer, I. Prager, D. Urlaub, M. Claus, R. Eils, J. Beaudouin, and C. Watzl. 2018. Single-Fluorescent Protein Reporters Allow Parallel Quantification of Natural Killer Cell-Mediated Granzyme and Caspase Activities in Single Target Cells. *Front. Immunol.* 9:1840. https://doi.org/10.3389/fimmu.2018.01840

Lopez, J.A., O. Susanto, M.R. Jenkins, N. Lukoyanova, V.R. Sutton, R.H. Law, A. Johnston, C.H. Bird, P.I. Bird, J.C. Whisstock, et al. 2013. Perforin forms transient pores on the target cell plasma membrane to facilitate rapid access of granzymes during killer cell attack. *Blood.* 121:2659–2668. https://doi.org/10.1182/blood-2012-07-446146

Mace, E.M., P. Dongre, H.T. Hsu, P. Sinha, A.M. James, S.S. Mann, L.R. Forbes, L.B. Watkin, and J.S. Orange. 2014. Cell biological steps and checkpoints in accessing NK cell cytotoxicity. *Immunol. Cell Biol.* 92:245–255. https://doi.org/10.1038/icb.2013.96

Malmberg, K.J., M. Carlsten, A. Björklund, E. Sohlberg, Y.T. Bryceson, and H.G. Ljunggren. 2017. Natural killer cell-mediated immunosurveillance of human cancer. *Semin. Immunol.* 31:20–29. https://doi.org/10.1016/j.smim.2017.08.002

Mariani, S.M., and P.H. Krammer. 1998. Differential regulation of TRAIL and CD95 ligand in transformed cells of the T and B lymphocyte lineage. *Eur. J. Immunol.* 28:973–982. https://doi.org/10.1002/(SICI)1521-4141(199803)28:03<973::AID-IMMU973>3.0.CO;2-T

Mariani, S.M., B. Matiba, C. Bäumler, and P.H. Krammer. 1995. Regulation of cell surface APO-1/Fas (CD95) ligand expression by metalloproteases. *Eur. J. Immunol.* 25:2303–2307. https://doi.org/10.1002/eji.1830250828

Medema, J.P., C. Scaffidi, F.C. Kischkel, A. Shevchenko, M. Mann, P.H. Krammer, and M.E. Peter. 1997. FLICE is activated by association with the CD95 death-inducing signaling complex (DISC). *EMBO J.* 16:2794–2804. https://doi.org/10.1093/emboj/16.10.2794

Moroso, V., H.J. Metselaar, S. Mancham, H.W. Tilanus, D. Eissens, A. van der Meer, L.J. van der Laan, E.J. Kuipers, I. Joosten, and J. Kwekkeboom. 2010. Liver grafts contain a unique subset of natural killer cells that are transferred into the recipient after liver transplantation. *Liver Transpl.* 16:895–908. https://doi.org/10.1002/lt.22080

Netter, P., M. Anft, and C. Watzl. 2017. Termination of the Activating NK Cell Immunological Synapse Is an Active and Regulated Process. *J. Immunol.* 199:2528–2535. https://doi.org/10.4049/jimmunol.1700394

Packard, B.Z., W.G. Telford, A. Komoriya, and P.A. Henkart. 2007. Granzyme B activity in target cells detects attack by cytotoxic lymphocytes. *J. Immunol.* 179:3812–3820. https://doi.org/10.4049/jimmunol.179.6.3812

Peter, M.E., and P.H. Krammer. 2003. The CD95(APO-1/Fas) DISC and beyond. *Cell Death Differ.* 10:26–35. https://doi.org/10.1038/sj.cdd.4401186

Prager, I., and C. Watzl. 2019. Mechanisms of natural killer cell-mediated cellular cytotoxicity. *J. Leukoc. Biol.* 105:1319–1329. https://doi.org/10.1002/JLB.MR0718-269R

Quan, L.T., M. Tewari, K. O'Rourke, V. Dixit, S.J. Snipas, G.G. Poirier, C. Ray, D.J. Pickup, and G.S. Salvesen. 1996. Proteolytic activation of the cell death protease Yama/CPP32 by granzyme B. *Proc. Natl. Acad. Sci. USA.* 93:1972–1976. https://doi.org/10.1073/pnas.93.5.1972

Rogers, C., T. Fernandes-Alnemri, L. Mayes, D. Alnemri, G. Cingolani, and E.S. Alnemri. 2017. Cleavage of DFNA5 by caspase-3 during apoptosis mediates progression to secondary necrotic/pyroptotic cell death. *Nat. Commun.* 8:14128. https://doi.org/10.1038/ncomms14128

Rouvier, E., M.F. Luciani, and P. Golstein. 1993. Fas involvement in Ca(2+)-independent T cell-mediated cytotoxicity. *J. Exp. Med.* 177:195–200. https://doi.org/10.1084/jem.177.1.195

Sandusky, M.M., B. Messmer, and C. Watzl. 2006. Regulation of 2B4 (CD244)-mediated NK cell activation by ligand-induced receptor modulation. *Eur. J. Immunol.* 36:3268–3276. https://doi.org/10.1002/eji.200636146

Schmidt, H., C. Gelhaus, M. Nebendahl, M. Lettau, C. Watzl, D. Kabelitz, M. Leippe, and O. Janssen. 2008. 2-D DIGE analyses of enriched secretory lysosomes reveal heterogeneous profiles of functionally relevant proteins in leukemic and activated human NK cells. *Proteomics.* 8:2911–2925. https://doi.org/10.1002/pmic.200800170

Schmidt, H., C. Gelhaus, M. Nebendahl, M. Lettau, R. Lucius, M. Leippe, D. Kabelitz, and O. Janssen. 2011. Effector granules in human T lymphocytes: proteomic evidence for two distinct species of cytotoxic effector vesicles. *J. Proteome Res.* 10:1603–1620. https://doi.org/10.1021/pr100967v

Srpan, K., A. Ambrose, A. Karampatzakis, M. Saeed, A.N.R. Cartwright, K. Guldevall, G.D.S.C. De Matos, B. Önfelt, and D.M. Davis. 2018. Shedding of CD16 disassembles the NK cell immune synapse and boosts serial engagement of target cells. *J. Cell Biol.* 217:3267–3283. https://doi.org/10.1083/jcb.201712085

Stinchcombe, J.C., and G.M. Griffiths. 2007. Secretory mechanisms in cell-mediated cytotoxicity. *Annu. Rev. Cell Dev. Biol.* 23:495–517. https://doi.org/10.1146/annurev.cellbio.23.090506.123521

Strasser, A., P.J. Jost, and S. Nagata. 2009. The many roles of FAS receptor signaling in the immune system. *Immunity.* 30:180–192. https://doi.org/10.1016/j.immuni.2009.01.001

Sutton, V.R., J.E. Davis, M. Cancilla, R.W. Johnstone, A.A. Ruefli, K. Sedelies, K.A. Browne, and J.A. Trapani. 2000. Initiation of apoptosis by granzyme B requires direct cleavage of bid, but not direct granzyme B-mediated caspase activation. *J. Exp. Med.* 192:1403–1414. https://doi.org/10.1084/jem.192.10.1403

Thiery, J., D. Keefe, S. Boulant, E. Boucrot, M. Walch, D. Martinvalet, I.S. Goping, R.C. Bleackley, T. Kirchhausen, and J. Lieberman. 2011. Perforin pores in the endosomal membrane trigger the release of endocytosed granzyme B into the cytosol of target cells. *Nat. Immunol.* 12:770–777. https://doi.org/10.1038/ni.2050

Urlaub, D., K. Höfer, M.L. Müller, and C. Watzl. 2017. LFA-1 Activation in NK Cells and Their Subsets: Influence of Receptors, Maturation, and Cytokine Stimulation. *J. Immunol.* 198:1944–1951. https://doi.org/10.4049/jimmunol.1601004

Vanherberghen, B., P.E. Olofsson, E. Forslund, M. Sternberg-Simon, M.A. Khorshidi, S. Pacouret, K. Guldevall, M. Enqvist, K.J. Malmberg, R. Mehr, and B. Önfelt. 2013. Classification of human natural killer cells based on migration behavior and cytotoxic response. *Blood.* 121:1326–1334. https://doi.org/10.1182/blood-2012-06-439851

Vrazo, A.C., A.E. Hontz, S.K. Figueira, B.L. Butler, J.M. Ferrell, B.F. Binkowski, J. Li, and K.A. Risma. 2015. Live cell evaluation of granzyme delivery and death receptor signaling in tumor cells targeted by human natural killer cells. *Blood.* 126:e1–e10. https://doi.org/10.1182/blood-2015-03-632273

Wang, Y., W. Gao, X. Shi, J. Ding, W. Liu, H. He, K. Wang, and F. Shao. 2017. Chemotherapy drugs induce pyroptosis through caspase-3 cleavage of a gasdermin. *Nature.* 547:99–103. https://doi.org/10.1038/nature22393

Watzl, C. 2014. How to trigger a killer: modulation of natural killer cell reactivity on many levels. *Adv. Immunol.* 124:137–170. https://doi.org/10.1016/B978-0-12-800147-9.00005-4

Wolchok, J.D., H. Kluger, M.K. Callahan, M.A. Postow, N.A. Rizvi, A.M. Lesokhin, N.H. Segal, C.E. Ariyan, R.A. Gordon, K. Reed, et al. 2013. Nivolumab plus ipilimumab in advanced melanoma. *N. Engl. J. Med.* 369:122–133. https://doi.org/10.1056/NEJMoa1302369

Zagury, D., J. Bernard, N. Thierness, M. Feldmann, and G. Berke. 1975. Isolation and characterization of individual functionally reactive cytotoxic T lymphocytes: conjugation, killing and recycling at the single cell level. *Eur. J. Immunol.* 5:818–822. https://doi.org/10.1002/eji.1830051205

Zhang, N., and M.J. Bevan. 2011. CD8(+) T cells: foot soldiers of the immune system. *Immunity.* 35:161–168. https://doi.org/10.1016/j.immuni.2011.07.010

Zhu, Y., B. Huang, and J. Shi. 2016. Fas ligand and lytic granule differentially control cytotoxic dynamics of natural killer cell against cancer target. *Oncotarget.* 7:47163–47172.